Our Heritage (UGC Care Listed)
ISSN: 0474-9030 Vol-68, Special Issue-12
National Conference on Recent Trends in Physics, Chemistry and Mathematics (RTPCM-2020)
Held on 4th February 2020
Organised by: Department of Physics, Chemistry and Mathematics, Sunderrao Solanke Mahavidyalaya, Majalgaon, MS

Magnetic Characterization Of Nano-Structured Cd-Substituted Cobalt Nanoferrite

***[1]C. M. Kale, [2]S. D. More, [3]S. K. Vyawahare, [4]K. M. Jadhav**

[1]Indraraj Art, Commerce, and Science College, Sillod Dist. Aurangabad
[2]Research Center, Deogiri College, Aurangabad
[3]Sunderrao Solunke Mahavidyalaya, Majalgaon. Dist. Beed
[4]Department of Physics, Dr. Babasaheb Ambedkar Marathwada University, Aurangabad (M.S.) India-431112

*Corresponding author: **cmkale1973@gmail.com**

Abstract

Ultrafine samples of the ferrite series $Co_{1-x}Cd_xFe_2O_4$ (where, x = 0.0, 0.1, 0.2, 0.3, 0.4, 0.5) synthesized by using Sol-Gel auto combustion method. X-ray analysis confirms the formation of a single-phase cubic spinel structure of all prepared samples. Using X-ray diffraction (XRD) analysis it is observed that, the lattice parameter increases with an increase in Cd^{2+} ions content x. It is due to the replacement of Co^{2+} by Cd^{2+} ions. The magnetic properties recorded at room temperature using a pulse-field magnetic hysteresis loop tracer. It is found that saturation magnetization (M_S), magneton number increases with an increase in Cd ions. The increase in Bohr magneton (n_B) number is associated with an increase in A-B interaction. Coercivity value decreases with cadmium content x, indicate that the prepared samples are in nanocrystalline nature.

Keywords: *Ferrite, Sol-Gel synthesis, X-ray diffraction, magnetic properties*

1. Introduction

Nanoscale polycrystalline ferrites with unique electrical and magnetic properties are of great interest to scientists and engineers [1, 2]. Transition metal oxides (MFe_2O_4) are

magnetic materials with cubic spinel structure and have been used in various electronic and electrical applications for the last decade. The high permeability in the radiofrequency region, make them suitable for use in electronic devices [3]. The high electrical resistivity and good magnetic properties make it an excellent core material for use in electronic and telecommunication applications [4].

The magnetic properties of ferrite materials can be changed by the substitution of various types of M^{2+} ions among divalent cations. The magnetic properties are linked with A-B interaction between the magnetic atoms on the tetrahedral (A) and octahedral [B] sites. Thus it is essential to know the distribution of cations over available tetrahedral (A) and octahedral [B] sites; to understand the magnetic properties of spinel ferrites. Improvements in saturation magnetization, electrical resistivity, and magnetic anisotropy can be achieved by a suitable method of preparation, proper atomic substitutions and careful sintering conditions [5]. From the application point of view, the most significant properties of magnetic materials, namely magnetic saturation, coercivity, magnetization, and loss, change drastically as the size of the particles moves down into the nanometric range [6, 7]. Among the different ferrites, nanosized cobalt cadmium ferrite [8] possesses attractive properties for application as soft magnets and low loss materials at high frequencies.

In the present investigation, cadmium substituted cobalt ferrite samples of the series $Co_{1-x}Cd_xFe_2O_4$ (where, x = 0.0, 0.1, 0.2, 0.3, 0.4, 0.5) were prepared by sol-gel auto combustion technique. Few reports are available to shows the effect of high-density cadmium cations substitution on the magnetic properties of cobalt ferrite [9]. This work aims to study the magnetic properties of cadmium substituted cobalt ferrite recorded at room temperature using a pulse-field magnetic hysteresis loop tracer. The substitution of cadmium in place of cobalt has been recommended because cadmium ions with their preferential occupancy to octahedral sites in the spinel lattice are known to develop high magnetic anisotropy. The influence of magnetic anisotropy with increasing high-density cadmium ions concentration may lead to improvements in magnetic properties.

2. Experimental

The ultrafine samples of the ferrite series $Co_{1-x}Cd_xFe_2O_4$ (where, x= 0.0, 0.1, 0.2, 0.3, 0.4, 0.5) prepared by using Sol-Gel auto combustion method. The starting samples were taken in the form of high purity, A. R. grade (>99%) nitrates such as Cobalt Nitrate, Cadmium Nitrate, and Ferric Nitrate. The molar ratio of metal nitrates to citric acid was taken as 1:3. The metal nitrates were dissolved together in a minimum amount of double distilled water to get a clear solution. An aqueous solution of citric acid was mixed with metal nitrates solution, then ammonia solution was slowly added to adjust the pH at 7. The mixed solution was kept on to a hot plate and the solution is continuously stirred at 90^0C. The obtained powder was then subjected to further heating treatment into a muffle furnace at a relatively low-temperature 400^0C for six hours. The final product is then ground and subjected to further study.

The steps of formation of ultrafine samples of the ferrite series $Co_{1-x}Cd_xFe_2O_4$ as shown in the flowchart **Fig.1**

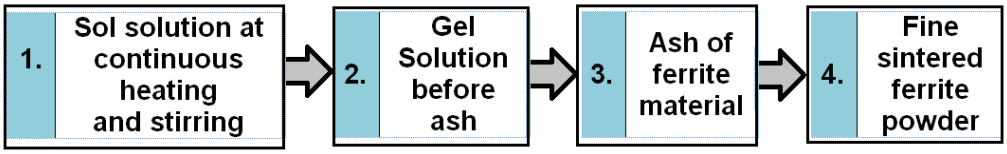

Fig.1. Flow chart for ferrite sample preparation by Sol-Gel auto combustion method

X-ray diffraction (XRD) patterns were recorded at room temperature in the 2θ range of 20^0 to 80^0 to confirm the formation of a single-phase cubic spinel structure. The magnetic properties of a material are studied by hysteresis loop tracer. Using hysteresis loops, the values of saturation magnetization (M_s), coercivity (H_c) and remanence magnetization (M_r) are obtained.

3. Results and discussion

3.1. X-ray diffraction analysis

X-ray diffraction (XRD) technique is used extensively for the characterization of the structure of surfaces and interfaces and crystal structures. The techniques, however, work on

the principle of Bragg diffraction law, $2d \sin\theta = n\lambda$. Fig. 2 shows a typical XRD pattern of, $Co_{0.7}Cd_{0.3}Fe_2O_4$ ferrite system.

Fig.2: XRD pattern of $Co_{0.7}Cd_{0.3}Fe_2O_4$ ferrite

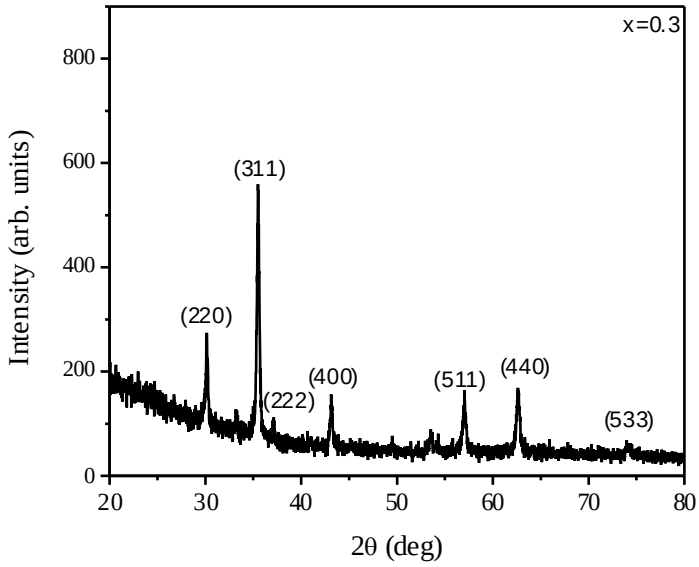

The XRD peak shows the sharp Bragg's peaks and there is no impurity peak observed. All the peaks are indexed by miller indices and it reveals that all the samples possess the single-phase cubic spinel structure. It is observed that the lattice parameter increases with an increase in Cd content 'x' as shown in Table.1. It is due to the replacement of smaller ionic radii atom Co^{2+} (0.82 A.U.) is replaced by larger ionic radii of Cd^{2+} (1.03 A.U.) [10].

Table.1: Lattice constant (a), saturation magnetization (M_S), remanance magnetization (M_r), coercivity (H_c) and Bohr magneton (nB) for $Co_{1+x}Cd_xFe_2O_4$ ferrite system

Cd content x	Lattice constant 'a' (Å)	Magnetic parameter				Bohr magneton 'nB'(μB)
		Mr (emu/gm)	Ms (emu/gm)	M_r: M_s	Hc (Oe)	
0.0	8.3652	76.22	74.86	1.018	1304.3	3.14
0.1	8.3662	67.58	79.73	0.848	1294.9	3.43

0.2	8.3738	73.00	80.46	0.907	1245.4	3.53
0.3	8.3840	65.43	82.80	0.790	1187.5	3.72
0.4	8.3951	71.02	93.26	0.762	954.22	4.43
0.5	8.3976	79.41	99.69	0.797	585.35	4.66

3.2. Magnetic Properties

The M-H loops provide the useful information about the magnetic parameters such as saturation magnetization (M_S), coercivity (H_C), remanence magnetization (Mr) and Bohr magneton (nB). The hysteresis plots (M-H) of typical samples x = 0.0, 0.1, 0.3 and 0.5 of $Co_{1-x}Cd_xFe_2O_4$ (where, x= 0.0, 0.1, 0.2, 0.3, 0.4, 0.5) ferrite system are depicted in **Fig. 3.**

The magnetic parameters such as saturation magnetization (M_S), remanence magnetization (M_r) and coercivity were obtained using the magnetization curve and are listed in **Table 1.**

3.2.1. The saturation magnetization (Ms)

The values of saturation magnetization (Ms) listed in Table.1. The first quadrants of the hysteresis curve show the variation of saturation magnetization (Ms) with Cd content x of the prepared $Co_{1-x}Cd_xFe_2O_{4)}$ ferrite system. The saturation magnetization (M_S) increases with cadmium content x, the increase in saturation magnetization is related to the magnetic moment of the constituent ions. The increase in Ms values may be due to the replacement of magnetic Co^{2+} by diamagnetic Cd^{2+} ions and because of this fact that A-B super-exchange interaction increases, leading to collapse magnetic properties.[11]

3.2.2. Remanence magnetization (Mr)

The remanence magnetization (Mr) of all the samples was obtained from M-H plots and the values are given in **Table 1.** Overall, the remanence magnetization shows less value than Ms and randomly orients as cadmium content x increases. The remanence magnetization values show that the prepared samples are nanocrystalline.

3.2.3. Remanence ratio (Mr: Ms)

The values Mr: Ms of the prepared samples are obtained from M-H plots and are shown in Table 1. The remanent ratio varies in between 0.7 to 1.0 for $0.0 \leq x \leq 1$. It is

Our Heritage (UGC Care Listed)
ISSN: 0474-9030 Vol-68, Special Issue-12
National Conference on Recent Trends in Physics, Chemistry and Mathematics (RTPCM-2020)
Held on 4th February 2020
Organised by: Department of Physics, Chemistry and Mathematics, Sunderrao Solanke Mahavidyalaya, Majalgaon, MS

observed that the remanent ratio almost decreases with an increase in cadmium content x. Further, it is noticed from the values of the remanence ratio shows a single domain state all the samples.

Fig.3: M-H loops of typical samples x = 0.0, 0.1, 0.3 and 0.5 of $Co_{1-x}Cd_xFe_2O_4$ ferrite system.

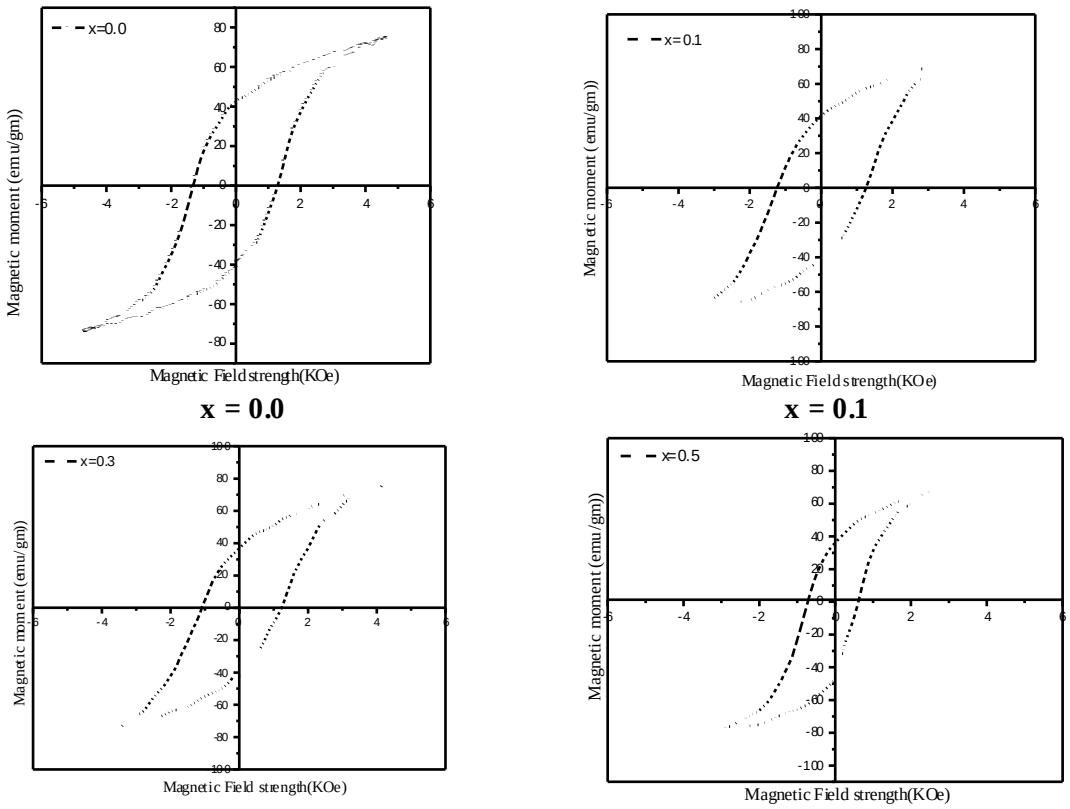

3.2.4. Magnetic moment (nB)

From Table.1, found that the magneton number increase with Cd-content x. The increase in Bohr magneton number is associated with the increase in A-B interaction. In ferrite, A-B interaction is dominant compared to A-A and B-B interaction. The substitution of diamagnetic Cd^{2+} ions in place of highly magnetic Co^{2+} ions results in strong in A-B interaction and hence nB increases. The magnitude of A-site magnetic moment decreases increasing the difference between A and B site moments so that nB increases

3.2.4. Coercivity

Using M-H plots the coercivity (Hc) of all the samples was obtained and the values are listed in **Table 1**. It is observed that coercivity value decreases with cadmium content x. The decrease in coercivity is related to a decrease in crystallite size concludes that the prepared samples possess nanocrystalline nature [12].

Our experimental results on various magnetic parameters such as saturation magnetization, remanence magnetization, and coercivity are fairly agreed with the other nanocrystalline spinel ferrite.

Conclusions

The Nano-crystalline cadmium substituted cobalt ferrite $Co_{1-x}Cd_xFe_2O_4$ (where, x= 0.0, 0.1, 0.2, 0.3, 0.4, 0.5) system were synthesized successfully by using sol-gel auto combustion technique. The X-ray powder diffraction pattern shows the formation of the cubic spinel structure of all the samples. The lattice constant increases with a decrease in cadmium content x. Saturation magnetization, remanence field, coercivity and Bohr magneton number all vary with cadmium substitution and showed that the prepared samples are nanocrystalline nature which may be used for various applications.

References

1. I.I.S. Lim, P.N. Njoki, H.Y. Park, X. Wang, L. Wang, D. Mott, C.J. Zhong, Nanotechnology 19 (2008) 305-102

2. J. Philip, P.D. Shima, B. Raj, Applied Physics Letters 92 (2008) 043108.

3. Q. Li, Y. Wang, C. Chang, Journal of Alloys and Compounds 505 (2010) 523

4. E. Veena Gopalan, I.A. Al-Omari, D. Sakthi Kumar, Y. Yosida, P.A. Joy, M.R. Anantharaman, Applied Physics A 99 (2010) 497.

5. A.Sattar, H.M.El-Sayed, K.M.El-Shokrofy, J. Mater. Sci 42 (2007)149

6. D.D. Awschalom, D.P.D. Vincenzo, Physics Today 43, (1995)

7. J. Shi, S. Gider, K. Babcock, D.D. Awschalom, Science 271 (1996) 937

8. S. P. Dalawai, T. J. Shinde, A. B. Gadkari and P. N. Vasambekar, Bull. Mater. Sci., Vol. 36, 5(2013), 919-922.

9. Misbah-ul. Islam, K. A. Hushmi, M. U. Rana, Tabbas. Solid State Com., 121 (2002) 51

10. M. Siva Ram Prasad, B. B. V. S. V. Prasad , B. Rajesh , K. H. Rao, K. V. Ramesh, J. Magn. Magn. Mater. 323 (2011) 2115-2121

11. M. Guillot, J. OstorBro, A. Marchand, A. Barle, Journal De Physique 12, 49 (1988) 923

12. M. Torikul Islam, S. S. Sikder, M. A. Hakim, Saroaut Noor and D. K. Saha, Journal of Engineering Science 05(1), 2014, 35-40

Our Heritage(UGC Care Listed)
ISSN: 0474-9030 Vol-68, Special Issue-12

National Conference on Recent Trends in Physics, Chemistry and Mathematics (RTPCM-2020) Held on 4th February 2020 Organised by: Department of Physics, Chemistry and Mathematics, SunderraoSolanke Mahavidhyalaya, Majalgaon, MS

Photoluminescence Study Of Ce^{3+} Activated Blue Emitting $Lisio_3:Ce^{3+}$ Lamp Phosphors

V.R.Panse[1], S.K.Vyawahare[2], D.B.Zade*[3] ,N.S.Kokode[4]

[1]Department of Physics, Late.B.S.Arts, Prof.N.G.Science & A.G.Commerce College Sakharkherda-443202, India

[2]Department of Physics, Sunderrao Solanke Mahavidyalaya, Majalgaon, Beed-India

*[3]Department of Physics, JSPM College Dhanora-India

[4]N.H.College,Bramhapuri, Gondwana University,Gadchiroli-441206,India

*[3]*Corresponding Author:* dbzade04@gmail.com

Abstract

Because of the spectroscopic properties of Ce^{3+} with favorable response and the ability to integrate the Ce^{3+} ion into diverse host inorgnaic material which was activated with cerium ion cover transformed interest for most of the applications . Therefore, with the suport of outstanding luminescence properties, inorganic materials activated with Ce^{3+} ions are applied in lightings industries, detectors with display systems for ionizing radiation .Here synthesis and photoluminescence (PL) investigation of $LiSiO_3:Ce^{3+}$ carried out using combustion synthesis method. The structural and morphological studies and confirmation of phase and purity were done using XRD and SEM. PL spectra of Ce^{3+} due to the 4f–5d transition of Ce^{3+} ions peaking at 332 nm. The photoluminescence emission spectra of $LiSiO_3:Ce^{3+}$ phosphor exhibit blue emission band centered at 440 nm. Usually, configuration of Ce^{3+} ion in ground state is divide into two levels viz., $^2F_{5/2}$ and $^2F_{7/2}$ whereas the $5d^1$ excited configuration is divide by the crystal playing field ranging from 2 to 5 components

Keywords:- Photoluminescence , XRD, SEM,CIE

Introduction

Cerium ions can be stabilized in host material in trivalent oxidation state. The stabilization and incorporation of Ce ions in the sample was studied and confirmed by the investigations of luminescence. Because of the spectroscopic properties of Ce^{3+} with favorable response and the ability to integrate the Ce^{3+} ion into diverse host inorgnaic material which was activated with cerium ion cover transformed interest for most of

the applications [1]. These materials recombine with high light capitulate, constructive emission wavelength, faster fluorescence decay with stability of temperature which make them attractive for useful in detectors for elevated energy physics [3] and also medical imaging [2]. Therefore, with the suport of outstanding luminescence properties, inorganic materials activated with Ce^{3+} ions are applied in lightings industries, detectors with display systems for ionizing radiation [3]. To calculate the 5d energies of another rare earth ion in same host lattices material trivalent cerium ion also is used as a reference ion [4]. So, the spectroscopic properties investigation of trivalent cerium ion in various host material is important for both the actual applications and the fundamental research. Generation of white light either by combination of basic fundamental colors or corresponding colors due to white light obtained from UV-blue LED by covering on LED suitable inorganic phosphors excitable by LED lights, For such inorganic phosphor transformed LED generating white light concluding development of suitable phosphor materials.

Experimental

The Ce^{3+} activated $LiSiO_3$ phosphor were prepared via combustion synthesis method. The starting AR grade materials (99.99% purity) were taken as follows: All ingredients used in the synthesis are of analytical reagent grade. Phosphors were synthesized by high temperature solid-state method. Silicate samples were obtained from the raw materials of metal carbonates with silicic acid ($SiO_2.9H_2O$), $LiCO_3$ and Tb_4O_7 which were stoichiometrically weighed out. All the ingredients were mixed according to stochiometric ratio in agate mortar and crushed it for 60 minutes to form a pasty solution , the solution was then transferred to silica crucible and kept inside a muffle furnace which is maintained at a constant temperature 800^0C for 24hrs duration. For preparing various activated phosphors, appropriate metal carbonates was added in the desired quantity to the starting material and similar procedure was followed. X-ray diffraction patterns were recorded on Philips PAN analytical X'pert Pro diffractometer Cu line (1.54056˚ A) was used.

Results and discussion

X-ray diffraction pattern

. It is carefully observed X ray diffraction pattern of the prepared $LiSiO_3$ host material compound does not shows any existence or subsistence of other raw material which is not direct confirmation of formation of desired compound. It is found that the XRD pattern of $LiSiO_3$ phosphor is well matched with standard JCPDS data file available i.e 83-1517 which shows that the final host product obtained is in crystalline and consistent homogeneous forms.

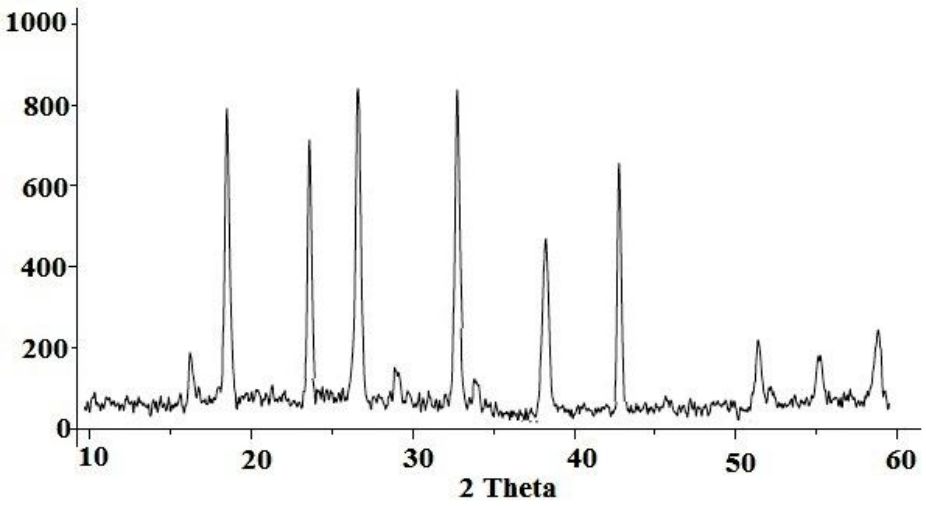

Fig.1 XRD-pattern of $LiSiO_3$ lamp phosphors.

Morphology of the combustion synthesized $LiSiO_3$ phosphors

Scanning electron microscopy (SEM) study was carried out to investigate the surface morphology and crystallite sizes of the synthesized phosphor powder.[5] Figure 2 shows the SEM micrograph of the prepared powder sample. Most of the particle is like foam shape. The shape of the phosphor influenced by the host and the activator also. The SEM micrograph of the $LiSiO_3$ powder phosphor was checked and the particle size allocation of the prepared phosphor is having significant potential application for lamp industries.

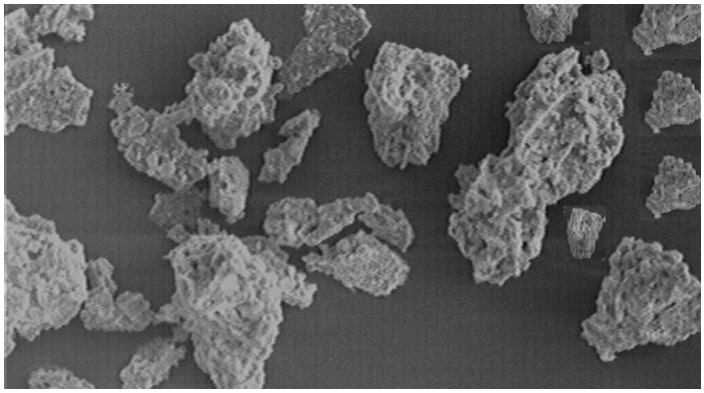

Fig. 2 Morphology of the combustion synthesized $LiSiO_3$ phosphors.

Ce^{3+} luminescence in $LiSiO_3$ phosphors

Fig. 3 and 4 shows photoluminescence excitation and emission spectra of $LiSiO_3$:Ce^{3+} phosphors which shows a wide absorption band in the range of 280 to 380 nm due to the 4f–5d transition of Ce^{3+} ions peaking at 332 nm. The photoluminescence emission spectra of $LiSiO_3$:Ce^{3+} phosphor as shown in fig exhibit blue emission band centered at 440 nm. Usually, configuration of Ce^{3+} ion in ground state is divide into two levels viz., $^2F_{5/2}$ and $^2F_{7/2}$ whereas the $5d^1$ excited configuration is divide by the crystal playing field ranging from 2 to 5 components. In this research work, the emission spectra of the prepared samples shows broad blue emission band in the range of 400-650 nm peaking at 440 nm. In accordance to the literature review [6] it is recognized to the transition of electron from the excited state of ^2D_J to the Ce^{3+} ions ground states viz.,$^2F_{5/2,7/2}$ of in the prepared $LiSiO_3$:Ce^{3+} host materials, the doublet characteristic of trivalent cerium ion not observed in the emission spectra. These photoluminescence emission spectrum resulting from the spectral overlaping of different emissions peaks connected with trivalent cerium ions substituted for five Sr sites in the T segment[58]. The excitation takes place among the maximum ground level spliting to the 5d levels while the emission developing from the excited level i.e. lowest level toward the two spliting ground levels state. Because of this for trivalent cerium ion, there are additional 4f–5d absorption bands in the PLE spectra while the 5d-4f emission observed in the photoluminescence emission spectrum is a representative double-band profile. The 5d-4f emission spectra of trivalent cerium ion which based strongly on the crystalographic

field. The trivalent cerium ion emission frequently is in the ultra-violet or blue spectral section although shifted toward green to yellow region (eg. $Y_3Al_5O_{12}:Ce^{3+}$), with the manipulation of the crystallographic surroundings. Usually, the characteristic emission trivalent cerium ions in a specific lattice site happen as doublet bands with the transitions observed due to the relaxed lowest 5d state of excitation to the ^2F_J (J=5/2,7/2) spin–orbit spliting 4f ground state.The separation of energy of the two bands corresponding to the common spin–orbit splitting up of (2000 cm^{-1}). The peak of excitation, which was expressed by the difference of energy of the lowest 5d level of excitation of trivalent cerium ion (332 nm) in the current Sr^{2+} host material compared with the free trivalent cerium ion (6.118 eV) , In present case as explaning in fig 6.22 and 6.23 .The emission spectra is clearly from the same observable site. The nine-fold synchronization Sr^{2+} is observed with Cs symmetry in a indistinct tri-capped trigonal prismatic geometry. Thus $LiSiO_3:Ce^{3+}$ among blue emission is able to find potential applications as a blue emitting lamp phosphor.

The compounds $LiSiO_3:Ce^{3+}$ was synthesized by modified wet chemical synthesis method and activated by alkaline earth Ce^{3+} ion , varies from 1 to 10 mol % with respects to corrosponding host material. The crest emission wavelengths of the prepared fluoride aluminates based compared with compounds prepared by high temperature reaction are summarized through emission spectrum graphical representation. It is going to investigated that, our prepared $LiSiO_3:Ce^{3+}$ blue emitting phosphor gives in the emission spectra at 440 nm exhibiting a blue shift moderately with commercial available phosphor and have prospective applications for blue lamp lighting industries.

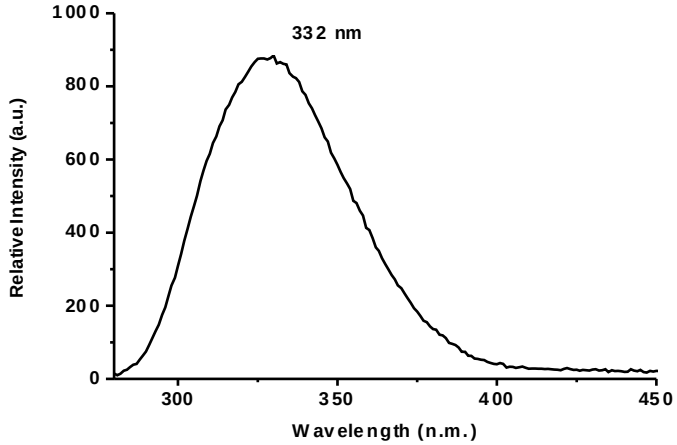

Fig. 3 Excitation Spectra for $LiSiO_3:Ce^{3+}$ phosphors, λ_{em}= 440 nm.

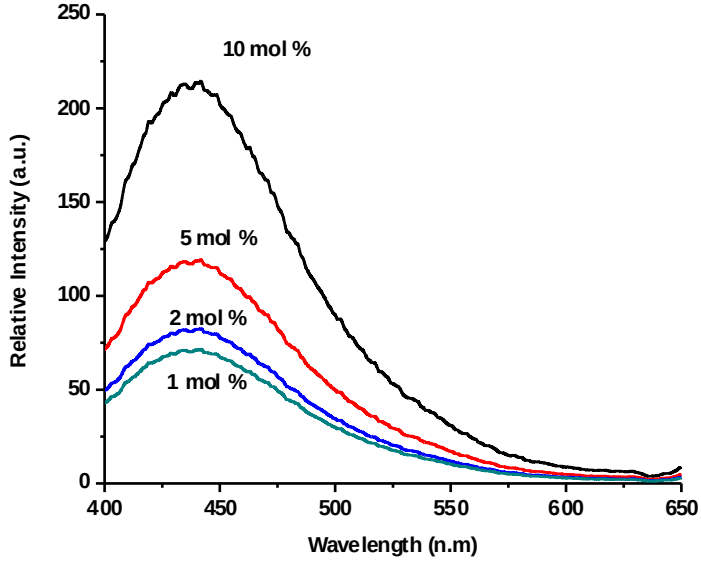

Fig. 4 Emission spectra for $LiSiO_3:Ce^{3+}$ phosphor λ_{ex}=332 nm

Chromatic properties of $LiSiO_3:Ce^{3+}$ phosphor

Herewe determine the coordinate of chromaticity indexed with the help of the emission spectra of Ce^{3+}. In 1931 chromaticity coordinate illustration invented by a renowned Commission of International de l'Eclairage (CIE) .It is the two dimensional graphical

pictorial illustration of any visible color by the eye system of human being on the x and y axis. [7] Generally illumination of lighting means colors referring lighting in conditions of the chromatic color coordinate which recognizes by the human being visualization scheme which use 03 major colors: i.e. blue ,red and green [3]. The CIE chromaticity diagram of $LiSiO_3:Ce^{3+}$ blue emitting phosphor shown in Fig 6.25. The color coordinates of the $LiSiO_3:Ce^{3+}$ phosphor observed, in blue region (C_x =0.234 C_y =0.035) phosphor is also in blue region shown in Fig 5.

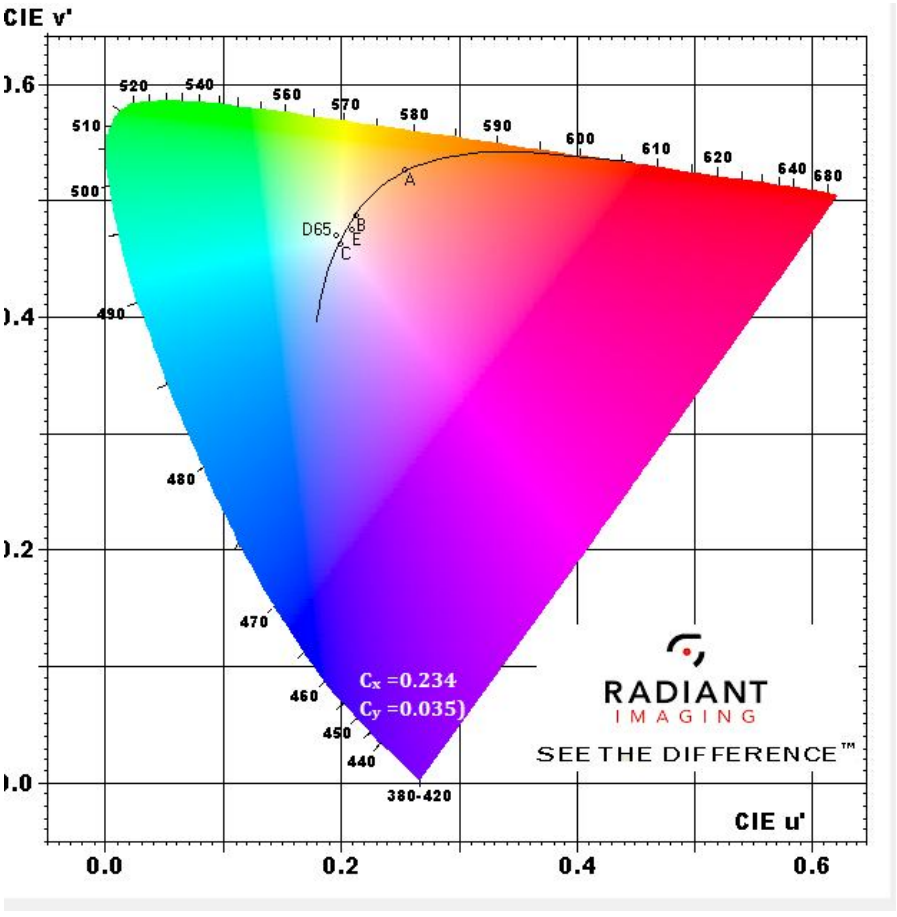

Figure5 : CIE chromatic diagram for $LiSiO_3:Ce^{3+}$ phosphor.

Because of the rising consequence of Ce^{3+} activated $LiSiO_3:Ce^{3+}$ with attractive blue emitting optical properties, which compose the prepared inorganic blue emitting phosphor become the exceptional prospective candidate for blue emitting phorphor industrial applications. The system of chromaticity coordinates (x, y) calculated with

the help of the color calculator program radiant imaging. The leading wavelength of the spectrum is the singular wavelength of monochromatic light which appear to have the samilar color as the light source. Such a wavelength calculated with the help of by sketching a singular line exclusive of delay from one end of the chromaticity white illuminants (0.31, 0.32) through the coordinates of x and y axes to be calculated, in anticipation of the line intersect the outer area locus point subsequently to the boundary of the spectral region of 1931 C.I.E. chromatic graphical representation [5].The result indicated from the spectrum in figure 6.25 is plotted by the Commission of Internationale de l'´Eclairage (CIE) 1931 chromaticity graphical representation.

6.4.4. Conclusion

1) The study of the photoluminescence characteristics of trivalent cerium activated blue-emitting $LiSiO_3:Ce^{3+}$ phosphors in the near UV–vis range shows the excitation bands at 332 nm.
2) Emission characteristics of $LiSiO_3:Ce^{3+}$ shows emission band at 440 nm, because of the corrosponding energy level.
3) The influence of activator concentration level on the photoluminescence properties of $LiSiO_3:Ce^{3+}$ phosphor realize in conditions of a smaller changes in relativistic intensity variation of the $5d\text{-}^2F_{5/2}$ to $5d\text{-}^2F_{7/2}$ ascribed to conceit and improved spliting of crystaografic field.

References

[1] P. Dorenbos, J. Lumin. 104 (2003) 239.

[2] K. Riwotzki, H. Meyssamy, H. Schnablegger, A. Kornowski, et al., Angew. Chem. Int. Ed. 40 (2001) 573.

[3] R.S. Ningthoujam, V. Sudarsan, S.V. Godbole, A.K. Tyagi, et al., Appl. Phys. Lett. 90 (2007) 173113.

[4] C.R. Ronda, J. Alloys Compd. 225 (1995) 534

[5] V.R. Panse, N.S. Kokode, K.N. Shinde, S.J. Dhoble, J. of Results in Physics 8 (2018) 99–103